

NON-LINEAR SPACE-PERIODIC DYNAMO IN AN ABC-FORCED MAGNETOHYDRODYNAMIC SYSTEM

O. M. Podvigina¹

International Institute of Earthquake Prediction Theory
and Mathematical Geophysics,
79 bldg. 2, Varshavskoe ave., 113556 Moscow, Russian Federation

Laboratory of General Aerodynamics, Institute of Mechanics,
Lomonosov Moscow State University,
1, Michurinsky ave., 119899 Moscow, Russian Federation

Observatoire de la Côte d'Azur, CNRS UMR 6529,
BP 4229, 06304 Nice Cedex 4, France

Centro de Matemática Aplicada da Universidade do Porto,
135 Rua das Taipas, 4050-600, Porto, Portugal

Submitted to Physica D

Abstract

Non-linear behavior of an MHD system with ABC forcing under periodic boundary conditions is considered. Most computations are performed for a fixed kinematic Reynolds number and magnetic Reynolds numbers increasing from 0 to 60. The kinematic Reynolds number is small enough for the trivial solution with a zero magnetic field to be stable to velocity perturbations. At the critical magnetic Reynolds number for the onset of instability of the trivial solution the dominant eigenvalue of the kinematic dynamo problem is real. In agreement with the bifurcation theory new steady states with non-vanishing magnetic field appear in this bifurcation. Subsequent bifurcations are investigated. A regime is detected, where chaotic variations of the magnetic field direction (analogous to magnetic field reversals) are observed in the temporal evolution of the system.

Key words: nonlinear magnetic dynamo, bifurcations, reversals

¹E-mail: olgap@mitp.ru

1 Introduction

The MHD system of equations is invariant under the symmetry preserving flows v and changing the sign of magnetic fields b :

$$h : (v; b) \rightarrow (-v; -b) \quad (1)$$

Temporal behavior involving magnetic field reversals, similar to those of the Earth magnetic field, can develop in a system with such a symmetry. The following scenario can be anticipated. Suppose for some values of a control parameter the system possesses a stable steady state, in which magnetic field vanishes. When the parameter varies, two steady states with a non-vanishing magnetic field emerge in a pitchfork bifurcation (generic to systems with the symmetry (1)). In subsequent bifurcations the steady states bifurcate into more complex attractors, remaining so far two distinct attractors related by (1). As the parameter varies further, the former attractors degenerate into invariant sets repelling in some directions, the attractor of the system becomes unique, and a trajectory on attractor jumps between the sets. Jumps involve changes in the magnetic field direction, and the resulting intermittency can thus be linked with the reversals. Our goal is to inspect, whether this scenario is feasible.

Reversals were observed in simulations of MHD systems with the geometry and boundary conditions corresponding to those of the Earth, see e.g. [1,2]. However, such computations are very demanding in CPU time, prohibiting numerical identification of complex bifurcations in that system.

We consider the Navier-Stokes equation

$$\frac{\partial v}{\partial t} = \nu \nabla^2 v + \frac{1}{R} v \cdot \nabla v - \nabla p + f \quad (2a)$$

and the magnetic induction equation

$$\frac{\partial b}{\partial t} = \nu \nabla^2 b + \frac{1}{R_m} b \cdot \nabla v \quad (2b)$$

under the solenoidality conditions

$$\nabla \cdot v = 0; \quad \nabla \cdot b = 0 \quad (2c)$$

Here v is flow velocity, b magnetic field, p pressure, R and R_m are kinematic and magnetic Reynolds numbers. (Since in the problem under consideration characteristic length and velocity magnitudes are of the order of unity,

the Reynolds numbers are defined as inverse viscosity and inverse magnetic diffusivity, respectively.) The fields are supposed to be 2-periodic in space.

The force

$$f = u_0 = R \quad (3)$$

is assumed, where u_0 is an ABC flow

$$u_0 = (A \sin x_3 + C \cos x_2; B \sin x_1 + A \cos x_3; C \sin x_2 + B \cos x_1): \quad (4)$$

For this force,

$$v = u_0; \quad b = 0 \quad (5)$$

is a steady solution to (2)–(4) for all Reynolds numbers.

This particular system is considered for the following reasons: First, space periodicity enables one to use pseudo-spectral methods [3–5], which are computationally less demanding than other numerical methods. Second, linear stability of the system (2)–(5) to hydrodynamic [6–8] and magnetic [9–12] perturbations was investigated both numerically and analytically (nonlinear regimes for some parameter values were also explored, see [7,8,12–14] and references therein). These studies provide guidance, in what parameter ranges the targeted type of behavior may be observed. In particular, growing magnetic modes exist for the flow (3) in broad intervals of constants A , B and C [10,11]. Third, since the critical magnetic Reynolds number is typically of the order of 10, only moderate R_m need to be considered, and a relatively low resolution (32^3 Fourier harmonics) suffices.

Magnetic field growth rates were calculated in [12] for the flow (4) with the coefficients satisfying $B = C$; $A^2 + B^2 + C^2 = 3$; $0 < B = A < 1$ for various values of R_m . For $R_m = 12$ there are three windows in $B = A$ of positive growth rates ([12], Fig. 2). We have checked that in the window $0.7 < B = A < 0.9$ the dominant eigenvalue is real, and in the other two windows it is complex. Distinct steady states with a non-zero magnetic field appear in a bifurcation of the trivial steady state (5), only if the magnetic induction operator has a zero (hence real) eigenvalue at the bifurcation point. This has suggested to set

$$A = 1; \quad B = C = 0.75; \quad (6)$$

these values of constants in (4) are assumed throughout.

In the present study we focus at non-hydrodynamic attractors. The hydrodynamic global stability of u_0 guarantees that magnetic field does not vanish

in saturated regime, if $v = u_0$ is a kinematic dynamo. We have verified that for $R = 4$, $v = u_0$ is a unique attractor of the hydrodynamic system (2.a, 2.c) with $b = 0$, and most computations are made for this value of R . Several runs are also performed for higher R .

A perturbation of the trivial steady state (5) with the energy of 10^{-6} in each Fourier harmonics spherical shell is employed as an initial condition. The range of existence of attractors is determined by continuation in parameter: the runs are done with an initial condition, which is a point on the attractor for close values of R_m .

2 Symmetries

The group of symmetries without inversion of time of an ABC flow with $B = C$, G , is comprised of two independent symmetries

$$s_1 : x_1 \rightarrow -x_1 ; x_2 \rightarrow x_2 ; x_3 \rightarrow x_3 ; t \rightarrow -t$$

$$s_2 : x_1 \rightarrow x_1 ; x_2 \rightarrow -x_2 ; x_3 \rightarrow -x_3 ; t \rightarrow -t$$

their superpositions

$$s_3 = s_2^2 : x_1 \rightarrow x_1 ; x_2 \rightarrow x_2 ; x_3 \rightarrow x_3 ; t \rightarrow t$$

$$s_4 = s_2^3 : x_1 \rightarrow x_1 ; x_2 \rightarrow -x_2 ; x_3 \rightarrow -x_3 ; t \rightarrow t$$

$$s_5 = s_1 s_2 : x_1 \rightarrow -x_1 ; x_2 \rightarrow -x_2 ; x_3 \rightarrow x_3 ; t \rightarrow -t$$

$$s_6 = s_1 s_2^2 : x_1 \rightarrow -x_1 ; x_2 \rightarrow x_2 ; x_3 \rightarrow -x_3 ; t \rightarrow t$$

$$s_7 = s_1 s_2^3 : x_1 \rightarrow -x_1 ; x_2 \rightarrow -x_2 ; x_3 \rightarrow -x_3 ; t \rightarrow -t$$

and the identity transformation $s_8 = e$ [7,15,16]. The group is isomorphic to the symmetry group of a square, D_4 .

Any symmetry of the force (3),(4) which does not involve inversion of time is also a symmetry of the Navier-Stokes equation (2.a) with $b = 0$. The group of symmetries of the MHD system (2)-(4),(6) is a direct product of G and the 2-element group Z_2 , generated by h (1). It has 16 elements, which are either s_i or $h s_i$.

Let A be an attractor of a dynamical system, invariant under a symmetry $g: g(A) = A$. Two cases can be distinguished: either A is pointwise invariant, i.e. $g(x) = x$ for all points $x \in A$, or it is invariant only as a set, with $g(x) \notin A$ for some $x \in A$. In what follows, only the symmetries for which an attractor is pointwise invariant are regarded as symmetries of the attractor.

Table 1. Attractors, detected for the MHD system with the forcing (3), (4), (6) for $R = 4$ and $0 < R_m < 60$. The third column shows the number of elements of the symmetry group for which an attractor is pointwise invariant, and the fourth { generators of the group.

R_m	Attractors	Number of symmetries	Generators
$R_m = 14$	steady state S_0	16	s_1, s_2, h
$15 < R_m < 24$	steady states $S_{1;ji}$ ($i = 1;2$)	8	hs_1, s_2
$25 < R_m < 37$	periodic orbits $P_{2;ji}$ ($i = 1;2$)	4	$hs_1, s_3 (= s_2^2)$
$37.5 < R_m < 38.5$	steady states $S_{1;ji}$ ($i = 1;2$)	8	hs_1, s_2
$39 < R_m < 39.2$	periodic orbits $P_{3;ji}^1$ ($i = 1;2$)	8	hs_1, s_2
$39.3 < R_m < 39.4$	periodic orbits $P_{3;ji}^2$ ($i = 1;2$)	8	hs_1, s_2
$R_m = 39.45$	periodic orbits $P_{3;ji}^4$ ($i = 1;2$)	8	hs_1, s_2
$R_m = 39.5$	chaotic $C_{1;ji} = P_{3;ji}^1$ ($i = 1;2$)	8	hs_1, s_2
$R_m = 39.6$	periodic orbits $P_{3;ji}^1$ ($i = 1;2$) & periodic orbit P_4	8 8	hs_1, s_2 hs_1, s_2
$39.7 < R_m < 41$	periodic orbit P_4	8	hs_1, s_2
$R_m = 42;43$	tori $T_{2;ji}$ ($i = 1;2$)	4	hs_1, s_3
$R_m = 45$	chaotic $C_{2;ji}$ ($i = 1;2$)	4	hs_1, s_3
$R_m = 46, 47$	chaotic $C_{3;ji}$ ($i = 1;4$)	2	hs_1
$R_m = 48, 49$	chaotic $C_{4;ji}$ ($i = 1;4$)	2	hs_1
$R_m = 50, 51$	chaotic $C_{5;ji}$ ($i = 1;2$)	2	hs_1
$52 < R_m < 58$	tori $T_{3;ji}$ ($i = 1;4$)	2	hs_1
$16 < R_m < 25$	periodic orbit P_1	4	hs_2
$26 < R_m < 60$	torus T_1	4	hs_2

3 Attractors of the MHD system for $R = 4$

Results of computations are summarized in Table 1. For $15 < R_m < 58$ the system under consideration possesses multiple attractors. For $16 < R_m < 58$ attractors, which we have detected, belong to two independent families; within each family they are genetically related by sequences of bifurcations. Attractors from different families have distinct groups of symmetries. The families can be distinguished also by their time-averaged kinetic (\overline{E}_k) and magnetic (\overline{E}_m) energies: $0.9 < \overline{E}_k < 1.1$, $0 < \overline{E}_m < 0.05$ for the first family, and $0.3 < \overline{E}_k < 0.7$, $0.07 < \overline{E}_m < 0.25$ for the second one.

The first family exists for $0 < R_m < 58$: the first attractor is the trivial steady state (S_0) remaining stable up to $R_m = 14$. It becomes unstable in a pitchfork bifurcation, in which two stable mutually symmetric steady states ($S_{1,1}$ and $S_{1,2}$) with a non-zero magnetic field emerge. The 8-element symmetry group of $S_{1,i}$ is isomorphic to D_4 ; however, it is distinct from G .

The second family emerges between $R_m = 15$ and $R_m = 16$: in addition to the steady states $S_{1,i}$, for $R_m > 16$ the system possesses another attractor, a stable periodic orbit P_1 . The orbit does not exist for $R_m = 15$; apparently it appears in a saddle-node bifurcation. For $R_m = 26$ the orbit is unstable and a torus T_1 has appeared in a Hopf bifurcation. T_1 remains an attractor for all higher considered R_m (specifically, for $R_m = 26, 27, 30, 40, 57$ and 60). For $R_m > 57$ the torus attracts trajectories (in the phase space) initially close to the trivial steady state S_0 , and for $R_m > 58$ it is the only global attractor of the system. The torus T_1 and the orbit P_1 were traced back from $R_m = 57$ by continuation in R_m . In what follows we will not discuss this family of attractors any more.

The steady states $S_{1,i}$ become unstable in a supercritical Hopf bifurcation at the interval $24 < R_m < 25$. A stable periodic orbit $P_{2,i}$ of period 12 appears in a vicinity of the steady state $S_{1,i}$. The two orbits are mutually symmetric (they are interrelated by (1)). Each periodic orbit possesses all 8 symmetries of its parent steady state, but each individual point of the orbit has a symmetry group of only 4 elements (it is isomorphic to D_2). At $R_m = 30$, after an initially small magnetic energy at first exponentially grows and afterwards decays with oscillations, it subsequently levels off (see a plateau about 400 time units long on Fig. 1a): the trajectory in the phase space evolves in a vicinity of $S_{1,i}$ (which is unstable now). In the further evolution the trajectory leaves the steady state, being attracted by $P_{2,i}$ (see Fig. 1b). The orbits exist for $25 < R_m < 37$ remaining attracting, and they disappear in a subcritical Hopf bifurcation between $R_m = 37$ and $R_m = 37.5$. For $R_m = 37.5, 38$ and 38.5 the two steady states $S_{1,i}$ are verified to be stable.

Next bifurcation of $S_{1,i}$ is again a supercritical Hopf bifurcation. The emerging mutually symmetric periodic orbits $P_{3,i}^1$, $i = 1; 2$ (one for each of

²This is consistent with results of [12]: since the ABC coefficients (6) are not normalized to satisfy $A^2 + B^2 + C^2 = 3$ as they are in [12], our Reynolds numbers are lower by a factor $(17=24)^{1=2}$.

the two steady states) possess all the symmetries of the steady states. For $39 < R_m < 39.2$ they are attracting, and their period is $(P_{3;i}^1) = 120$. Behavior of a sample trajectory in the phase space resembles the one shown on Fig. 1; however, on Fig. 2a the plateau corresponding to the evolution in the vicinity of the unstable steady state $S_{1;i}$ virtually disappears, and the period is much larger. The orbit is located in a different region of the phase space (cf. Fig. 1b and Fig. 2b). At an R_m between 39.2 and 39.3 two mutually symmetric orbits $P_{3;i}^2$ ($i = 1;2$) of a twice larger period emerge (see Fig. 3a). A sequence of period-doubling bifurcations begins. The next period doubling occurs at the interval $39.4 < R_m < 39.45$ (see period-four orbit $P_{3;i}^4$ for $R_m = 39.45$ on Fig. 3b). At $R_m = 39.5$ a trajectory, initially close to S_0 , is either already chaotic, or close to an orbit of a very long period $P_{3;i}^1$ (see Fig. 3c). This indicates that at $R_m = 39.5$ the period-doubling cascade is over. For $R_m = 39.6$ a trajectory with the same initial condition is attracted to a period-one orbit $P_{3;i}^1$.

Another attractor exists for $R_m = 39.6$. It reveals itself when the attractor for $R_m = 39.7$, which is unique in this region of the phase space (see below) is continued in smaller R_m . This is a periodic orbit P_4 , involving transitions between the two period-two orbits $P_{3;i}^2$ (see Fig. 4a). The orbit is invariant under $h(1)$ and any symmetry from G . In the course of temporal evolution, direction of magnetic field is reversed, behavior of non-zero magnetic field Fourier coefficients is similar to that shown on Fig. 4b. A reversal takes a relatively short time, during which initially the energy of magnetic field attains the minimum and kinetic (the maximum), and subsequently magnetic energy blows up to a maximum, with the kinetic energy simultaneously reaching its minimum (Fig. 4c,d). No attractor of this type is revealed by further continuation in smaller R_m .

This bifurcation is apparently of the following nature. In the period-doubling cascade inevitably many unstable periodic orbits $P_{3;i}^M$ ($i = 1;2$) of periods $(P_{3;i}^M) = M (P_{3;i}^1)$ are created. Consider two such orbits $P_{3;i}^m$ ($m = 2$ in our case) related by (1). Suppose that for some value of a control parameter the stable manifold of $P_{3;i}^m$ intersects the unstable manifold of $P_{3;i}^m$, and a heteroclinic trajectory connecting these orbits emerges. Consider the symmetry, which maps one of the periodic orbits to another. Under this symmetry the heteroclinic trajectory is mapped to a distinct heteroclinic trajectory, and the two form a heteroclinic cycle. The cycle may give rise to a periodic orbit

P_4 , when the control parameter varies. (This scenario is analogous to that in two-dimensional dynamical systems, where a homoclinic connection generically implies for close values of the control parameter existence of periodic orbits in a vicinity of the homoclinic trajectory, and their period tends to infinity when the critical value is approached.)

For $39.7 < R_m < 41$ sample trajectories, initially close to the trivial steady state S_0 , are attracted by the periodic orbit P_4 . However, while for $R_m = 39.6$ such a trajectory follows closely each of $P_{3,i}^2$ (Fig. 4a), this is not the case anymore for higher R_m (see Fig. 5). In agreement with our conjecture that appearance of the orbit is related to heteroclinic connection, the period decreases from 800 for $R_m = 39.7$ to 500 for $R_m = 41$.

For $R_m = 42$ and 43 the regime is quasi-periodic: the orbit P_4 bifurcates into two attracting tori $T_{2,i}$ ($i = 1; 2$) interrelated by (1) (see Fig. 6). The second frequency can be observed on Fig. 6a, showing real part of the Fourier component $b_{0,i,1}^3$ of magnetic field. The time average of this Fourier component is negative (Fig. 6a); hence, the symmetry (1) maps this attractor to a distinct one. (For $37.5 < R_m < 41$ the component vanishes, because former attractors P_4 for $39.6 < R_m < 41$, $P_{3,i}^m$ for $39 < R_m < 39.6$, and $S_{1,i}$ for $37.5 < R_m < 38.5$] possess the symmetry $hs_5 = hs_1s_2$.) Note qualitatively different behavior (Figs. 6a and 6b) of different Fourier coefficients of the magnetic field (for $R_m < 41$ all non-zero components evolved coherently).

For $R_m = 45$ two mutually symmetric attractors persist (Fig. 7): each torus $T_{2,i}$ bifurcates into a chaotic attractor $C_{2,i}$. Reversals are less regular, yet they are too ordered in comparison with those of the Earth's magnetic field.

For $R_m = 46$ (Fig. 8) behavior of a sample trajectory suggests existence of four (unstable) steady states $S_{2,i}$ (see plateaux at $1500 < t < 2100$). They are mutually symmetric, and have the same 4-element symmetry group generated by hs_1 and s_3 . Apparently two $S_{2,i}$'s emerged from each $S_{1,i}$ in a pitchfork bifurcation. Initially (at $0 < t < 700$) the sample trajectory for $R_m = 46$ undergoes several reversals, similar in nature to those observed for $39.7 < R_m < 45$. Afterwards it is attracted to a steady state $S_{2,i}$. Subsequent sample evolution consists of transitions between the steady state $S_{2,i}$ and the region of the phase space where a former chaotic attractor $C_{2,i}$ was located (duration of repeating events in the saturated regime is ≈ 1700). In particular, large-amplitude excursions at $2350 < t < 2500$, $2300 < t < 2450$, $4000 < t < 4150$, etc., are

rem iniscent of the behavior of a $C_{2;i}$ trajectory for $R_m = 45$. Thus, apparently two former chaotic attractors $C_{2;i}$ have disappeared in collision with the four steady states $S_{2;i}$ to give rise to four new chaotic attractors $C_{3;i}$. It is notable that the sample trajectory leaves a vicinity of the $S_{2;i}$ in alternating directions along the unstable manifold. For $R_m = 47$ the behavior is similar to the one at $R_m = 46$.

For $R_m = 48$ the system possesses four mutually symmetric attractors $C_{4;i}$. Events are longer than in the previous regime, about 3000 time units (see Fig. 9). They exhibit a new feature, a phase of initially exponentially decaying oscillations (e.g. at $1700 < t < 2300$ and $4500 < t < 5200$). This indicates existence of a weakly unstable periodic orbit of a new kind, $P_{5;i}$ ($i = 1;4$), in a vicinity of the former chaotic attractor $C_{3;i}$. A similar behavior is also observed for $R_m = 49$.

For $R_m = 50;51$ (Fig. 10) the four $C_{4;i}$ are superceded by two new attractors, $C_{5;i}$. Large amplitude oscillations, e.g. at $7500 < t < 8500$, are due to attraction of the trajectory by weakly unstable tori $T_{3;i}$ ($i = 1;4$), which have bifurcated from the periodic orbits $P_{5;i}$. In the saturated regime behavior consists of three phases: (i) a trajectory is close to a periodic orbit $P_{5;i}$ (e.g. at $2300 < t < 3000$ and $4300 < t < 5000$); (ii) the trajectory evolves in the vicinity of a torus $T_{3;i}$ (e.g. at $3200 < t < 4000$ and $5300 < t < 6000$); (iii) the trajectory abruptly jumps toward the second periodic orbit $P_{5;i^0}$ to reproduce the sequence of phases.

For $R_m = 52$ each of the two former chaotic attractors splits into two attracting tori $T_{3;i}$ (Fig. 11; cf. Figs. 10b and 11b). The four new attractors are mutually symmetric, they are stable for $52 < R_m < 58$.

For $57 < R_m < 60$ a sample trajectory initially close to S_0 is attracted by the torus T_1 .

4 Attractors of the M H D system for $R_m = 40$.

We do not perform analysis for other values of R in such detail, as for $R = 4$. Runs are made for $R_m = 40$ and only for several values of R with an initial condition, same for all runs, being a small perturbation of S_0 . The question we address is how the behavior changes with R , in particular, if reversals are present for higher R and whether magnetic field decays in saturated regime

Table 2. Attractors, detected for the MHD system with the force (3), (4), (6) for $R_m = 40$ and $3 \leq R \leq 25$. The third column shows the number of elements of the symmetry group for which an attractor is pointwise invariant, and the fourth { generators of the group.

R	Attractors	Number of symmetries	Generators	\overline{E}_k	\overline{E}_m
R = 3	T_1	4	hs_2	0.4	0.25
R = 4	chaotic P_4	8	hs_1, s_2	0.95	0.03
R = 6	chaotic $C_{2;i}$ ($i = 1; 2$)	4	hs_1, s_3	0.95	0.03
R = 10	periodic orbit P_6	8	hs_1, s_2	0.5	0.06
R = 15	chaotic C_6	4	s_1, s_3	0.6	0.04
R = 20	tori $T_{4;i}$ ($i = 1; 2$)	4	s_1, s_3	0.7	0.01
R = 25	chaotic $C_{7;i}$ ($i = 1; 2$)	1	e	0.5	0.02

Table 3. Attractors, detected for the hydrodynamic system (2.a) with the force (3), (4), (6) for $3 \leq R \leq 25$. The third column shows the number of elements of the symmetry group for which an attractor is pointwise invariant, and the fourth { generators of the group.

R	Attractors	Number of symmetries	Generators	\overline{E}_k
R = 3; 4; 6	u_{ABC}	8	s_1, s_2	1.06
R = 10	u_{ABC}	8	s_1, s_2	1.06
	S_1^h	8	s_1, s_2	0.99
R = 15	S_1^h	8	s_1, s_2	0.93
R = 20	chaotic C_1^h	4	s_2	0.9
R = 25	chaotic C_2^h	1	e	0.7

S_1^h for $R = 10$ was traced back from $R = 15$; it is not observed for $R = 6$.

for moderate R . Results of computations are summarized in Table 2. Computations with the same R and the same initial condition for the flow are also performed for the purely hydrodynamic system (2.a), in order to compare the temporal behavior and attractors of the two systems.

For $R = 3$ the detected attractor is the torus T_1 (which is an attractor for $R = 4$ and $26 \leq R_m \leq 60$). For $R = 6$ reversals take place, similar to those observed for $R = 4$ and $R_m = 45$, and the attractor is $C_{2;i}$. Thus, for R close to 4 no new attractors are found.

For $R = 10$ a new attractor was found in the full MHD system { a periodic orbit P_6 with a symmetry group of 8 elements. Comparison of Tables 2 and

3 reveals no relation of attractors of the hydrodynamic and MHD systems for $R = 10, 15$ and 20 . For these Reynolds numbers a small magnetic field (magnetic energy E_m is below 0.07 ; see Table 2) drastically changes behavior of the system { the hydrodynamic and MHD systems have attractors of different types, and the average kinetic energy \overline{E}_k decreases significantly, e.g. for $R = 20$ $\overline{E}_m = 0.01$ and \overline{E}_k decreases from 0.9 (the hydrodynamic case) to 0.7 (the MHD case).

For $R = 15$ behavior of the sample trajectory of the MHD system in saturated regime is chaotic. But before the saturated regime sets in, the trajectory is attracted by P_6 and for $1000 \leq t \leq 2000$ remains close to this periodic orbit (see Fig. 12), which is now weakly unstable. For $R = 20$ the trajectory with the same initial condition is attracted to a new torus $T_{4;i}$; initially the temporal behavior of the trajectory resembles the one observed for $R = 15$ (cf. Figs. 12 and 13).

For $R = 25$ the MHD system possesses new chaotic attractors $C_{7;i}$ ($i = 1; 2$) with a trivial symmetry group. They resemble the chaotic attractor C_6 observed for $R = 15$ (cf. Fig. 12 and Fig. 14), but unlike $C_{7;i}$, C_6 is unique and has a symmetry group of four elements. Comparison of $C_{7;i}$ with the attractor of the non-magnetic Navier-Stokes equation, which also is chaotic, reveals that the influence of magnetic field is in some sense stabilizing: Fourier coefficients of the flow experience fewer jumps and the amplitude of their oscillations is much smaller (compare Fourier components of flows on Figs. 14b and 15b). An exponential growth of the initially small magnetic field in the sample evolution of the system begins only at $t = 200$ (Fig. 14c). Accordingly, until $t = 300$ the flow evolution is similar to the one in the absence of magnetic field. Magnetic field starts growing, when the trajectory is attracted by a weakly unstable periodic orbit in the hydrodynamic subspace. Departure from this orbit causes an initial decay of magnetic field before the onset of saturated behavior.

For $R = 15$ and 20 behavior of Fourier components of magnetic field is similar to the one shown on Fig. 14d. It consists of chaotic irregular small-period oscillations about zero, quite different from the behavior observed for $R = 4$. Thus for $R_m = 40, 15 \leq R \leq 25$ the considered system is not in a regime resembling reversals.

5 Conclusion

Our computations show that magnetic field reversals are not an uncommon feature of a nonlinear dynamical system of magnetohydrodynamic type, at least in some region of parameter values. The dissimilarity with the Earth reversals is not very surprising, since we consider a simplified set of equations (neither account of thermal or sedimentation-driven convection is taken, nor that of the Coriolis force) in an idealized space-periodic geometry.

The bifurcation scenario leading to emergence of reversals, which we put forward, proved feasible. Reversals were found only for small R , for which the hydrodynamic system has a unique globally stable steady state. Complexity of the sequence of bifurcations obtained in simulations is comparable to that of the hydrodynamic system studied in [7,8]. Numerous types of behavior are identified, which involve a large variety of attractors and unstable invariant sets of various types influencing behavior of evolutionary solutions. Regime of reversals arises following merging of two distinct attractors, the underlying mechanism is apparently based on heteroclinic connection { we continue to investigate it.

An analytic study of other global bifurcations observed here is required, in particular, of how chaotic attractors C_{2ji} , C_{3ji} , C_{4ji} and C_{5ji} are related. It is desirable to make a more detailed numerical analysis of bifurcations occurring in the regions on the $(R; R_m)$ plane, which are not explored in the present work.

Acknowledgments

I am grateful to V. Zheligovsky for discussions. Part of this work was done at the Department of Mathematics, University of Exeter, UK, where I worked as visiting scientist in January { February, 2001. The visit was made possible through an invitation of Royal Society. Visits to the Observatoire de la Côte d'Azur were supported by the French Ministry of Education. A part of results were obtained using computational facilities provided by the program "Simulations Interactives et Visualisation en Astronomie et Mécanique (SIVAM)" at the Observatoire de la Côte d'Azur. The work was concluded during a visit to Departamento de Matemática Aplicada, Faculdade de Ciências, University of Porto, Portugal at the kind invitation of Centro de Matemática Aplicada in June { July, 2001.

References

- [1] Glatzmaier G. A. and Roberts P. H. A three-dimensional self-consistent computer simulation of a geomagnetic field reversal. *Nature* 377 (1995), 203–209.
- [2] Sarson G. R. and Jones C. A. A convection driven geodynamo reversal model, *Phys. Earth Planet. Int.* 111 (1999), 3–20.
- [3] Gottlieb D. and Orszag S. A. Numerical Analysis of Spectral Methods, SIAM CBMS (NSF Regional Conference Series in Applied Math. (1977).
- [4] Canuto C., Hussaini M. Y., Quarteroni A. and Zang T. A. Spectral Methods in Fluid Dynamics, Springer-Verlag, Berlin (1988).
- [5] Boyd J. P. Chebyshev & Fourier Spectral Methods, Springer-Verlag, Berlin (1989).
- [6] Galloway D. J. and Frisch U. A note on the stability of a family of space-periodic Beltrami flows, *J. Fluid Mech.* 180 (1987) 557–564.
- [7] Podvigina O. and Pouquet A. On the non-linear stability of the 1:1:1 ABC flow, *Physica D* 75 (1994), 471–508.
- [8] Podvigina O. M. Spatially-periodic evolutionary and steady solutions to the three-dimensional Navier-Stokes equation with the ABC-force. Institute of Mechanics, Lomonosov Moscow State University (1999).
- [9] Arnold V. I. and Korkina E. I. The growth of a magnetic field in a three-dimensional incompressible flow, *Vestnik Moscow State Univ., Ser. Math.* 3 (1983) 43–46 (in Russian).
- [10] Galloway D. J. and Frisch U. Dynamical action in a family of flows with chaotic streamlines, *Geophys. Astrophys. Fluid Dynamics* 36 (1986), 53–83.
- [11] Childress S. and Gilbert A. D. Stretch, twist, fold: the fast dynamo, Springer-Verlag, Berlin (1995).
- [12] Galanti B., Sukem P. L. and Pouquet A. Linear and Non-Linear Dynamics Associated With ABC Flows, *Geophys. Astrophys. Fluid Dynamics* 66 (1992), 183–208.
- [13] Feudel S., Seehafer N. a., Galanti B. and Schmidtmann O. Symmetry breaking bifurcation for the magnetohydrodynamic equation with helical forcing, *Phys. Rev. E* 54 (1996), 2589–2596.

[14] Brummel N. H., Cattaneo F. and Tobias S. M. Linear and nonlinear dynamo properties of time-dependent ABC flows, *Fluid Dyn. Res.* 28 (2001), 237–265.

[15] Arnold V. I. On the evolution of magnetic field under the action of advection and diffusion, in *Some problems of modern analysis* (ed. V. M. Tikhomirov), Moscow Univ. Press (1984) 8–21 (in Russian).

[16] Dombre T., Frisch U., Greene J. M., Henon M., Mehr A. and Soward A. Chaotic stream lines in the ABC flows, *J. Fluid Mech.* 167 (1986), 353–391.

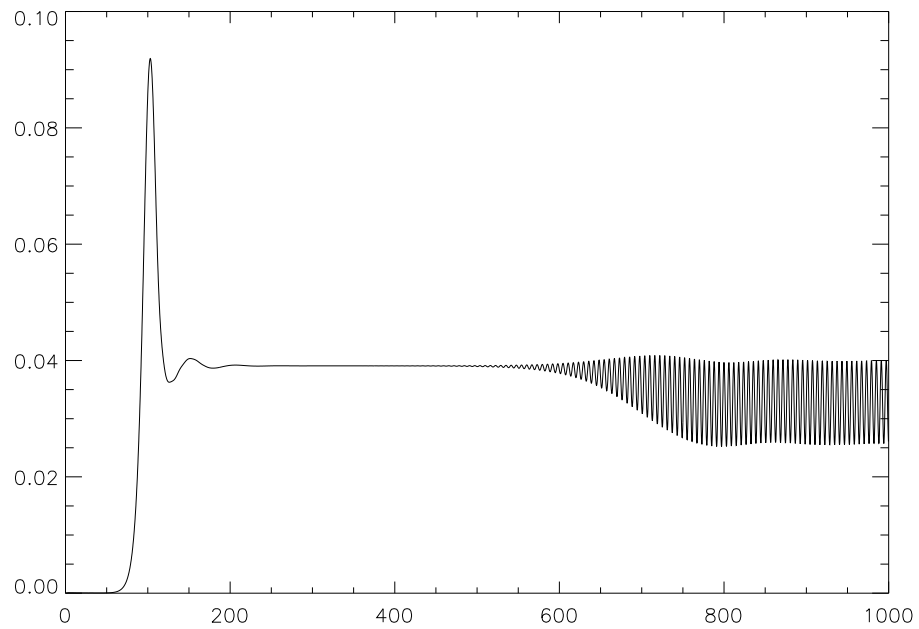


Figure 1a. Magnetic energy (vertical axis) as a function of time (horizontal axis) for $R = 4$ and $R_m = 30$.

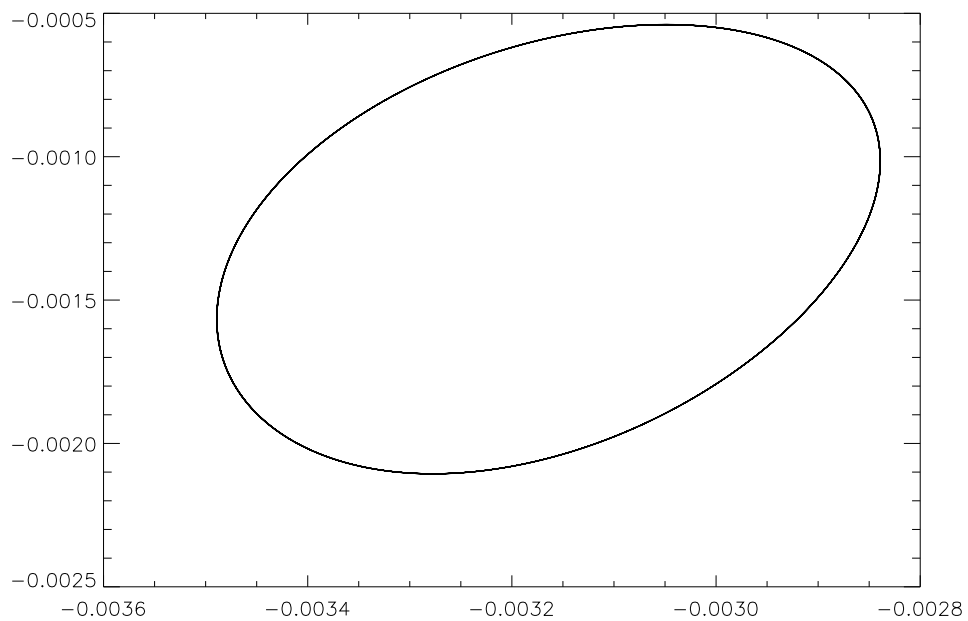


Figure 1b. Projection of the trajectory in saturated regime (a periodic orbit $P_{2,i}$) on the plane of Fourier coefficients $\text{Im } b_{0,1,2}^1$ (horizontal axis) and $\text{Re } v_{0,1,2}^1$ (vertical axis) for $R = 4$ and $R_m = 30$ (same run as on Fig. 1a).

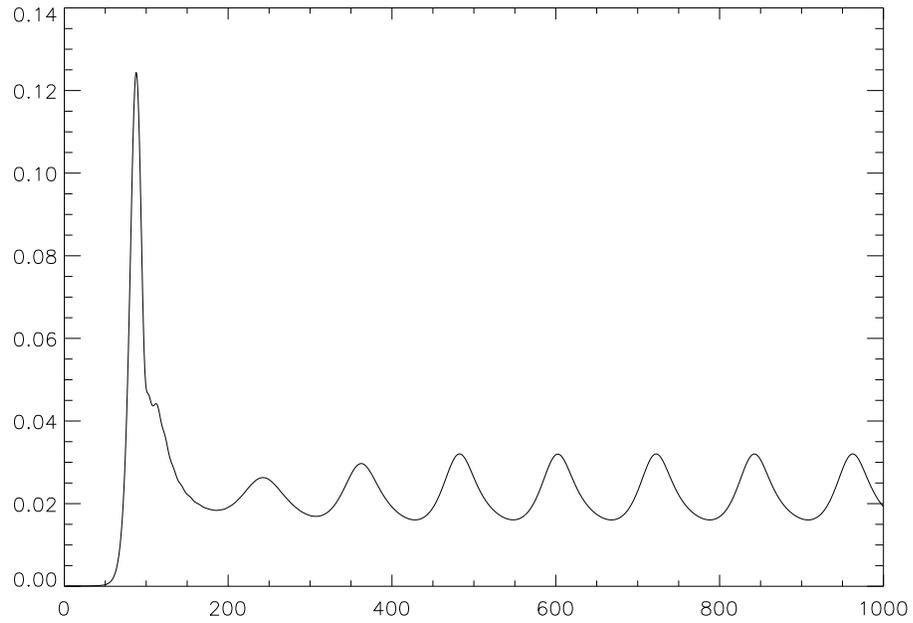


Figure 2a. Magnetic energy (vertical axis) as a function of time (horizontal axis) for $R = 4$ and $R_m = 39.2$.

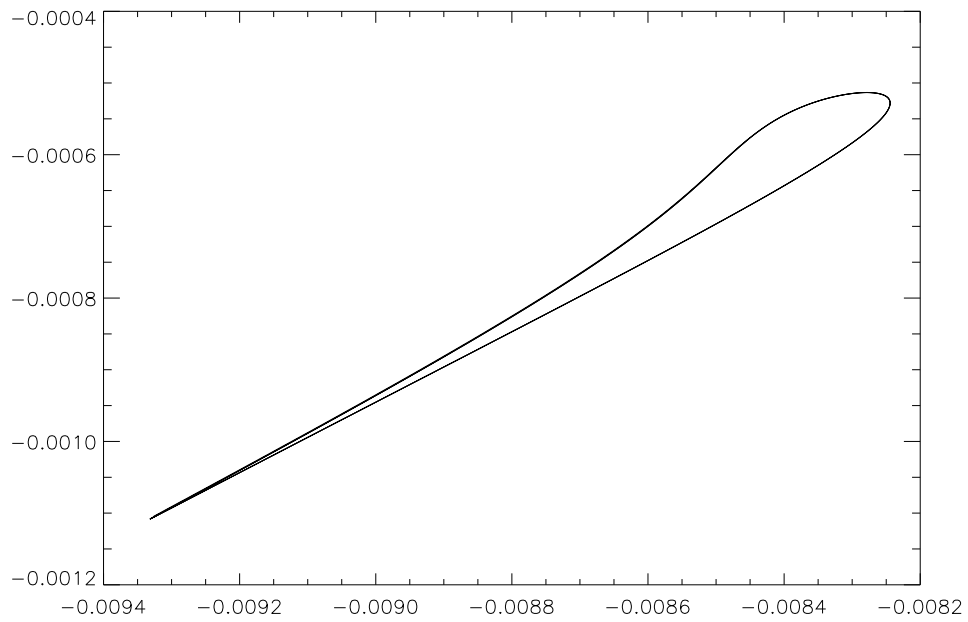


Figure 2b. Projection of the trajectory in saturated regime (a periodic orbit $P_{3;1}^1$) on the plane of Fourier coefficients $\text{Im } b_{0;1,2}^1$ (horizontal axis) and $\text{Re } v_{0;1,2}^1$ (vertical axis) for $R = 4$ and $R_m = 39.2$ (same run as on Fig. 2a).

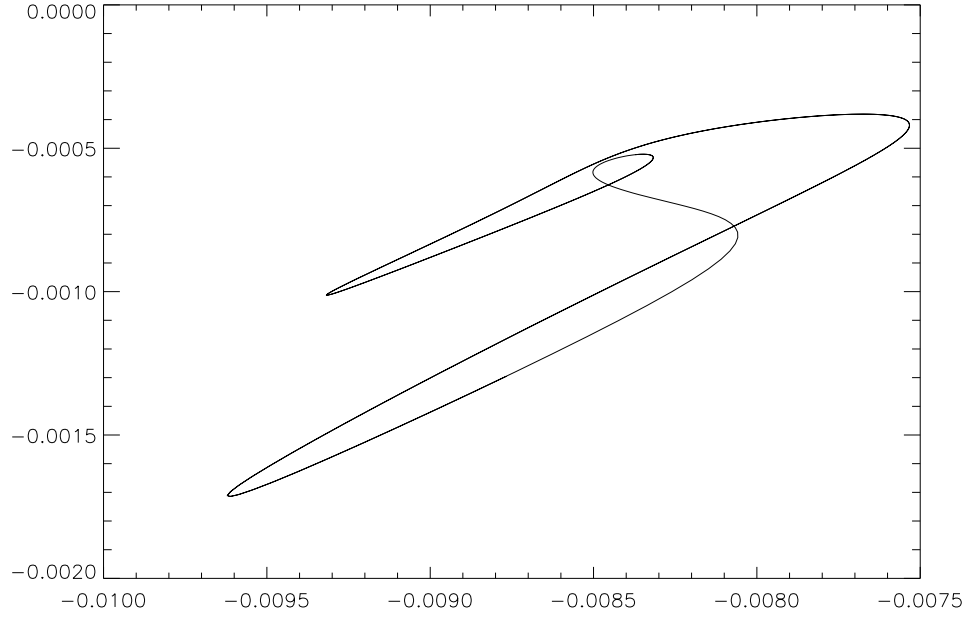


Figure 3a. Projection of the trajectory in saturated regime (a periodic orbit $P_{3;i}^2$) on the plane of Fourier coefficients $\text{Im } b_{0;1;2}^1$ (horizontal axis) and $\text{Re } v_{0;1;2}^1$ (vertical axis) for $R = 4$ and $R_m = 39:4$.

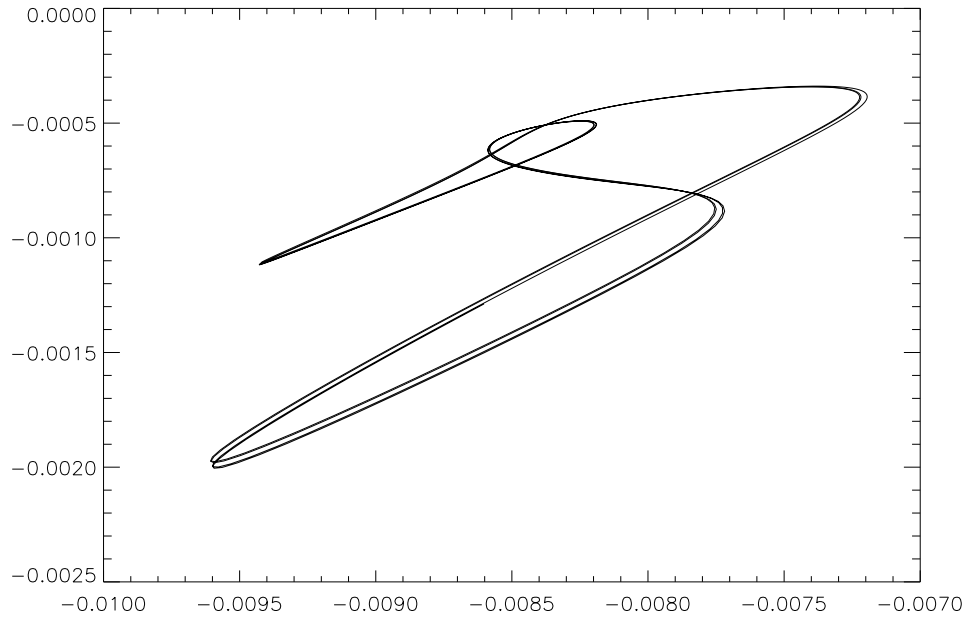


Figure 3b. Projection of the trajectory in saturated regime (a periodic orbit $P_{3;i}^4$) on the plane of Fourier coefficients $\text{Im } b_{0;1;2}^1$ (horizontal axis) and $\text{Re } v_{0;1;2}^1$ (vertical axis) for $R = 4$ and $R_m = 39:45$.

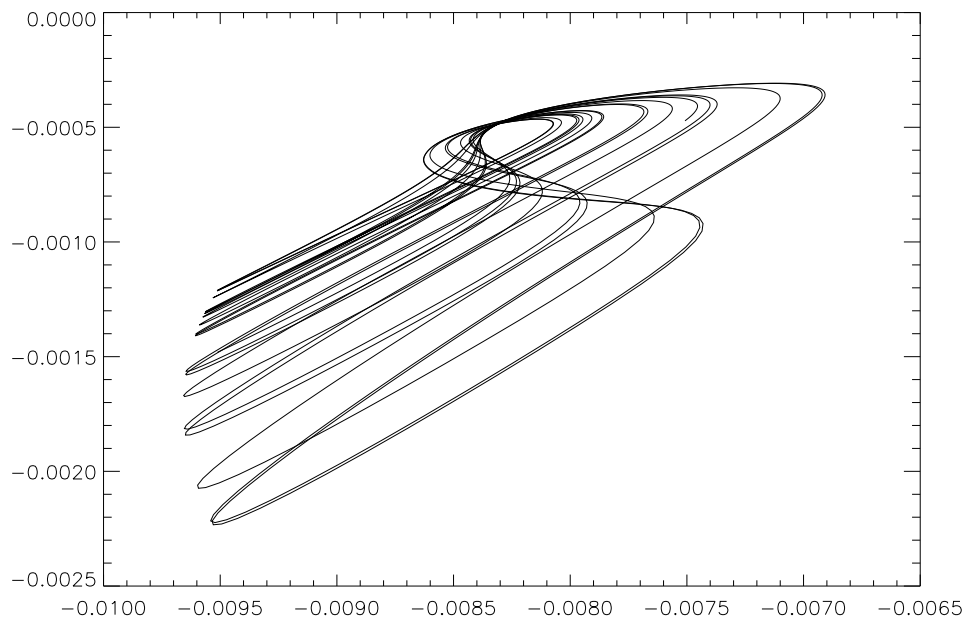


Figure 3c. Projection of the trajectory in the phase space in saturated regime (a periodic orbit $P_{3;l}^1$) on the plane of Fourier coefficients $\text{Im } b_{0;l;2}^1$ (horizontal axis) and $\text{Re } v_{0;l;2}^1$ (vertical axis) for $R = 4$ and $R_m = 39.5$.

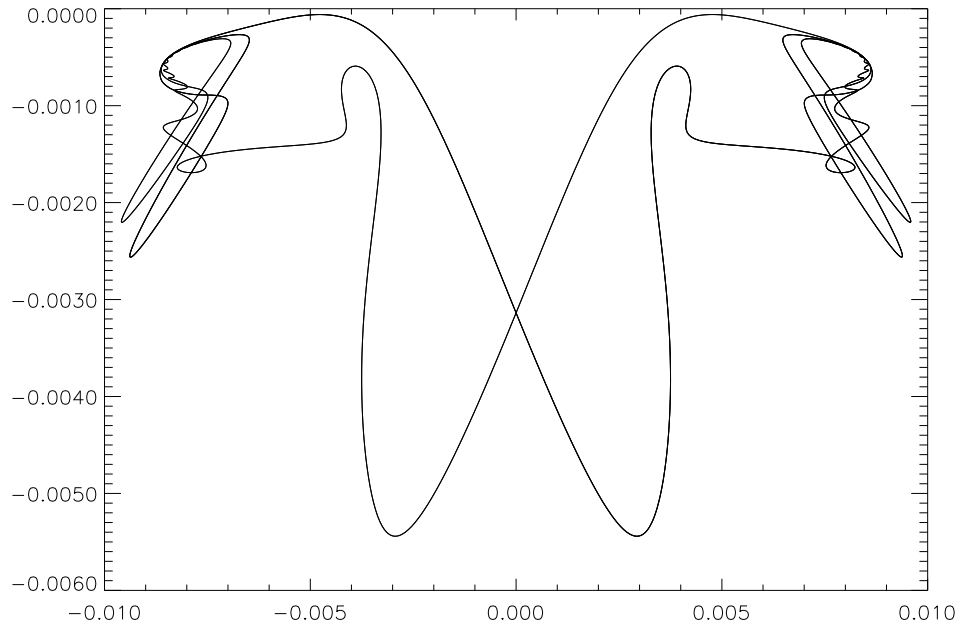


Figure 4a. Projection of the trajectory in saturated regime (periodic orbit P_4) on the plane of Fourier coefficients $\text{Im } b_{0;l;2}^1$ (horizontal axis) and $\text{Re } v_{0;l;2}^1$ (vertical axis) for $R = 4$ and $R_m = 39.6$.

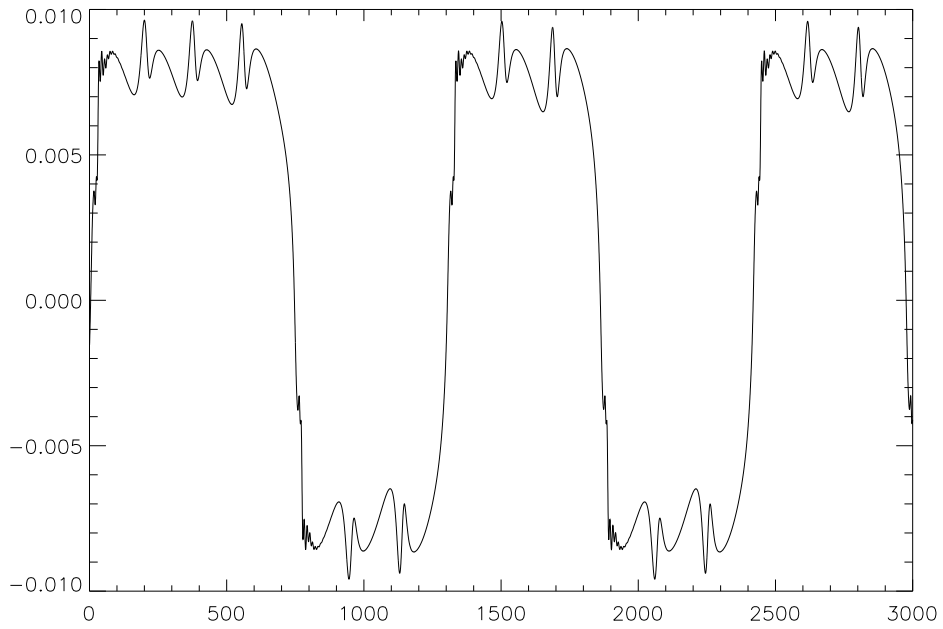


Figure 4b. Fourier coefficient $\text{Im } b_{0;l;2}^1$ (vertical axis) as a function of time (horizontal axis) for $R = 4$ and $R_m = 39.6$ (same run as on Fig. 4a).

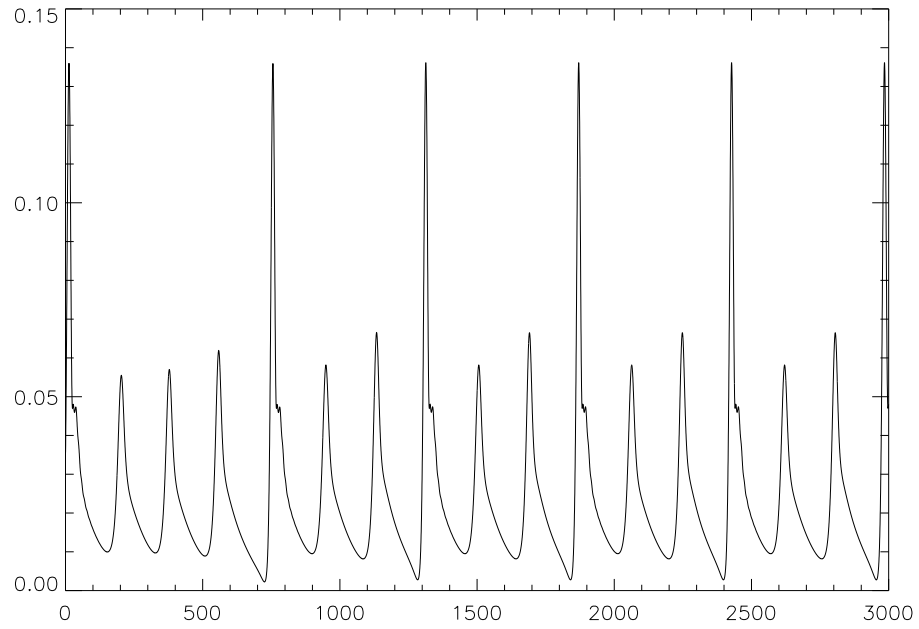


Figure 4c. Magnetic energy (vertical axis) versus time (horizontal axis) for $R = 4$ and $R_m = 39:6$ (same run as on Fig. 4a).

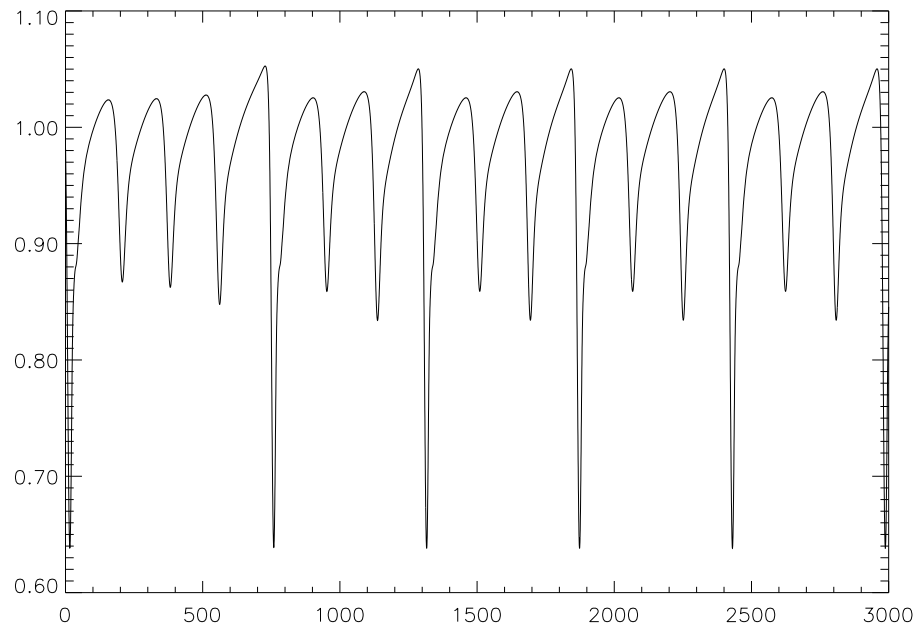


Figure 4d. Kinetic energy (vertical axis) versus time (horizontal axis) for $R = 4$ and $R_m = 39:6$ (same run as on Fig. 4a).

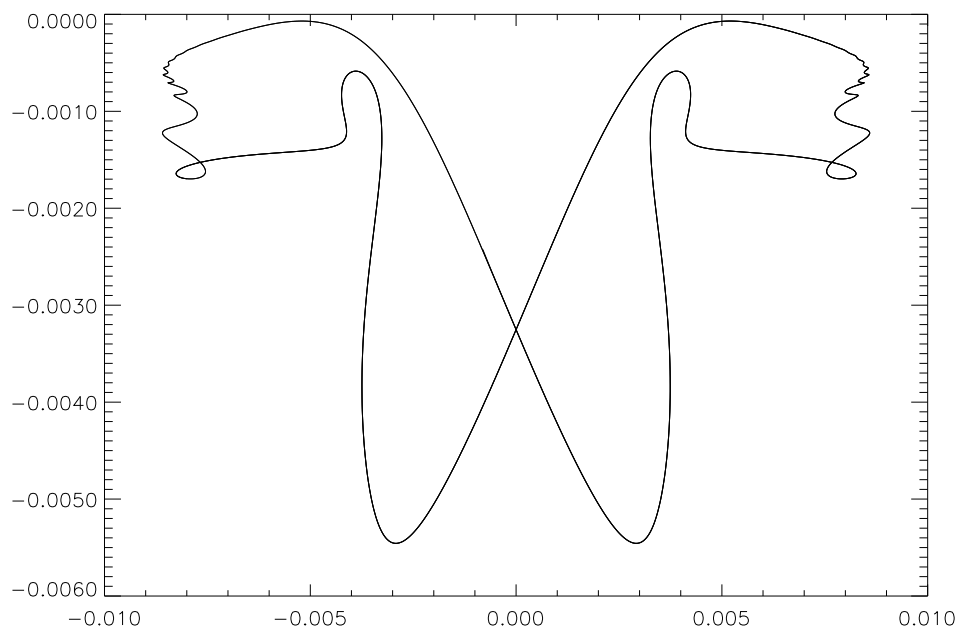


Figure 5. Projection of the trajectory in saturated regime (periodic orbit P_4) on the plane of Fourier coefficients $\text{Im } b_{0;1,2}^1$ (horizontal axis) and $\text{Re } v_{0;1,2}^1$ (vertical axis) for $R = 4$ and $R_m = 39:7$.

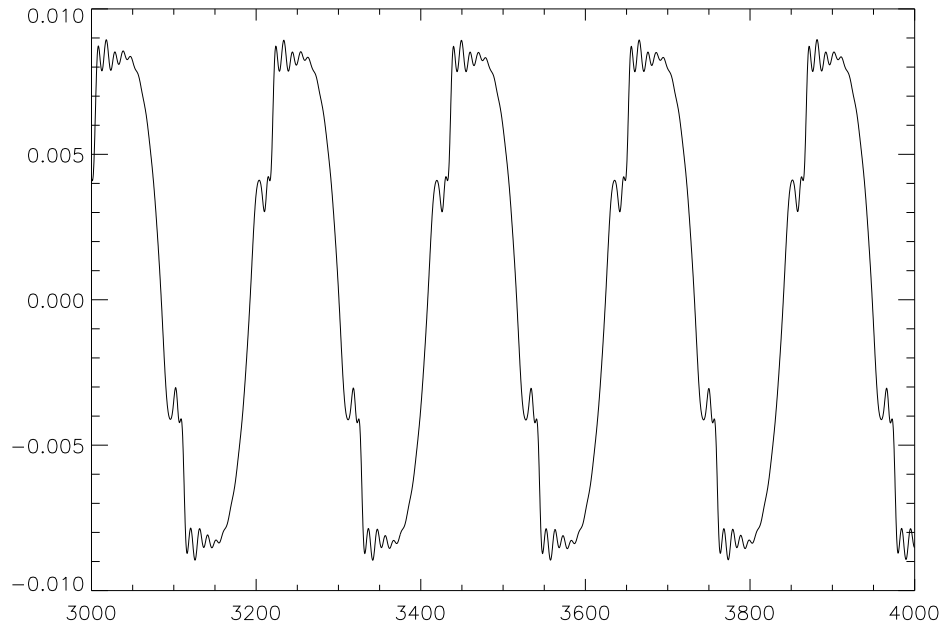


Figure 6a. Fourier coefficient $\text{Im } b_{0,1,2}^1$ (vertical axis) as a function of time (horizontal axis) for $R = 4$ and $R_m = 42$.

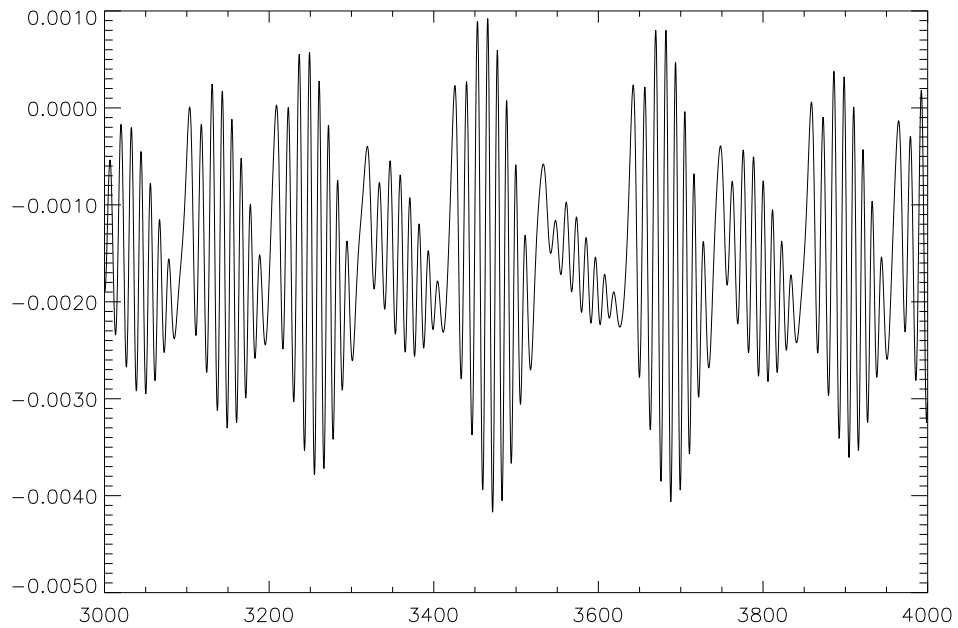


Figure 6b. Fourier coefficient $\text{Re } b_{0,1,1}^3$ (vertical axis) as a function of time (horizontal axis) for $R = 4$ and $R_m = 42$ (same run as on Fig. 6a).

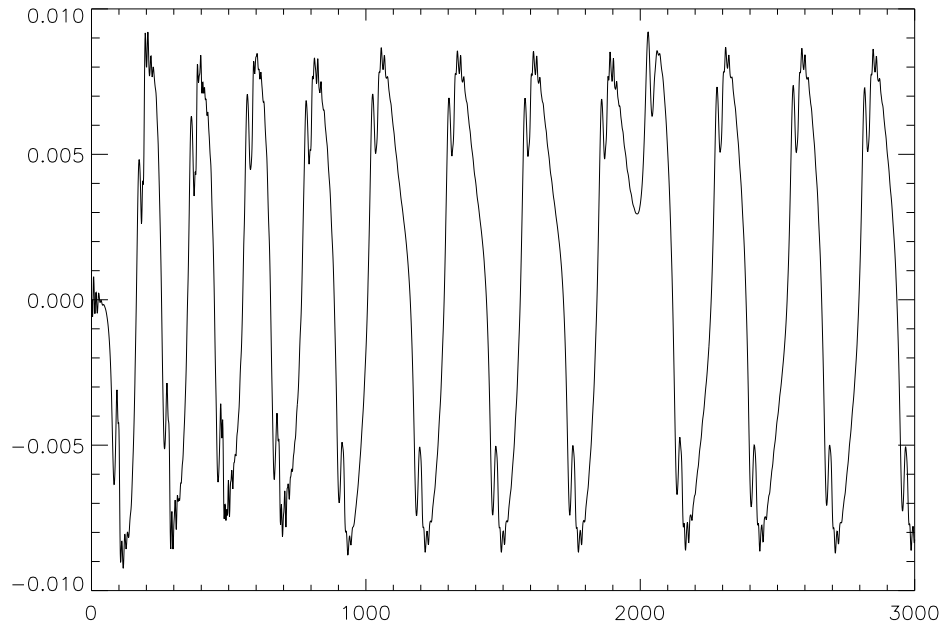


Figure 7a. Fourier coefficient $\text{Im } b_{0,1,2}^1$ (vertical axis) as a function of time (horizontal axis) for $R = 4$ and $R_m = 45$.

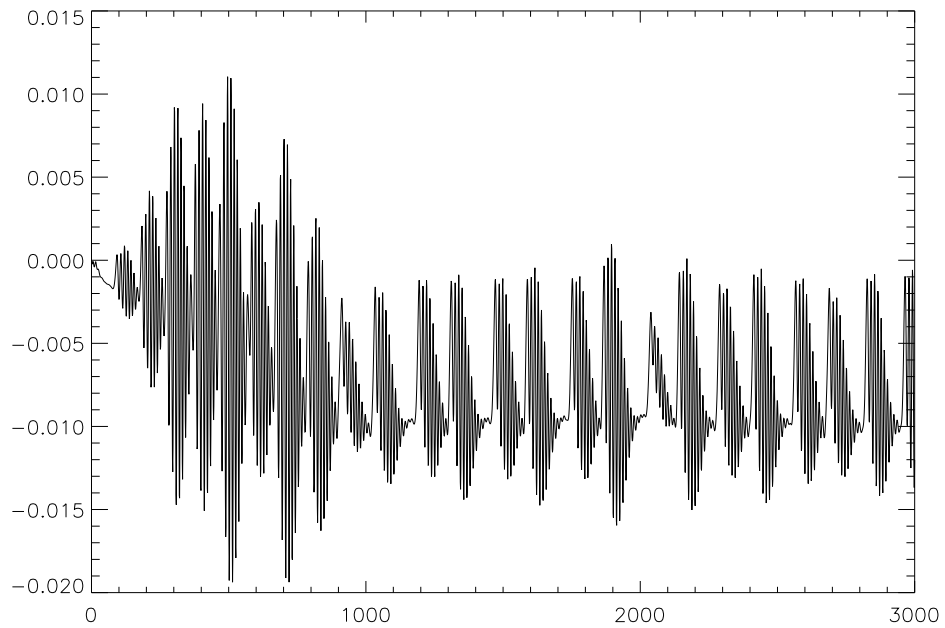


Figure 7b. Fourier coefficient $\text{Re } b_{0,1,1}^3$ (vertical axis) as a function of time (horizontal axis) for $R = 4$ and $R_m = 45$ (same run as on Fig. 7a).

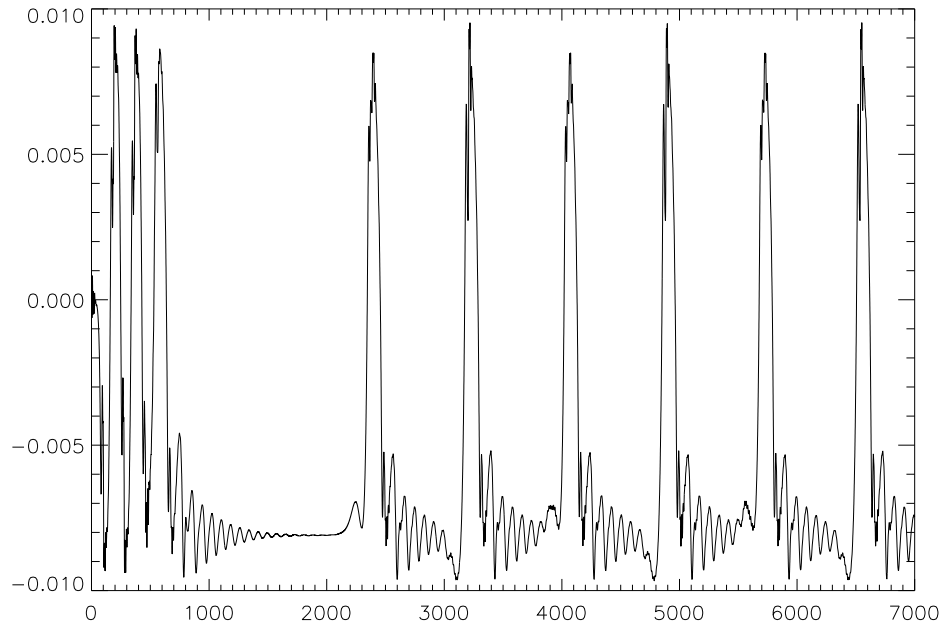


Figure 8a. Fourier coefficient $\text{Im } b_{0,1,2}^1$ (vertical axis) as a function of time (horizontal axis) for $R = 4$ and $R_m = 46$.

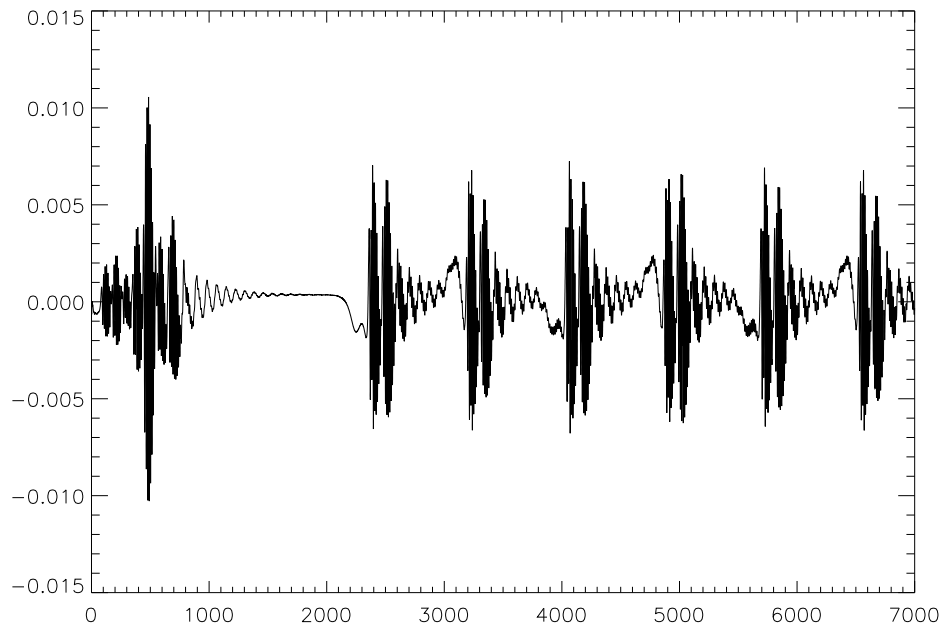


Figure 8b. Fourier coefficient $\text{Re } b_{0,1,1}^3$ (vertical axis) as a function of time (horizontal axis) for $R = 4$ and $R_m = 46$ (same run as on Fig. 8a).

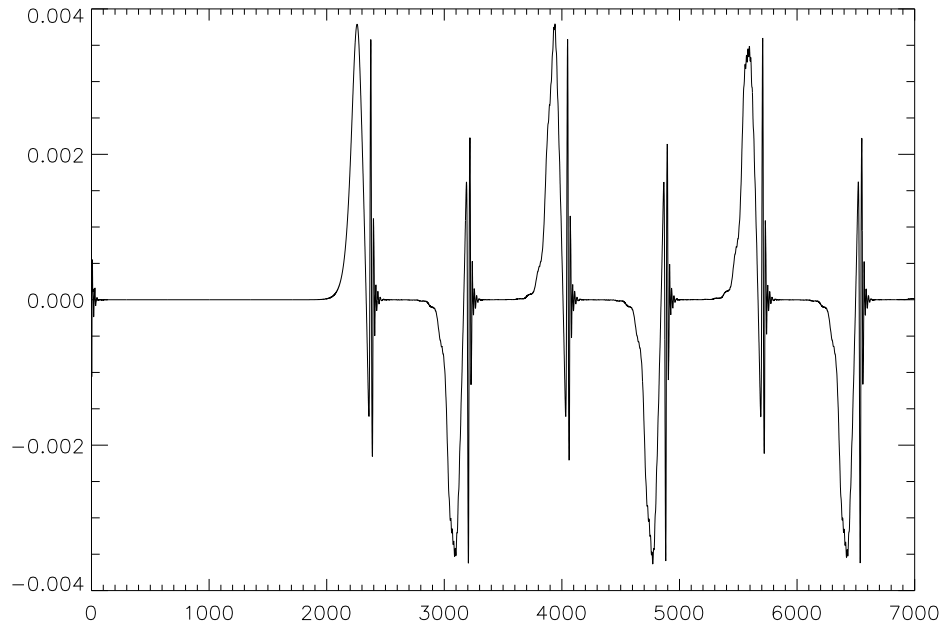


Figure 8c. Fourier coefficient $\text{Re } b_{1;0;1}^3$ (vertical axis) as a function of time (horizontal axis) for $R = 4$ and $R_m = 46$ (same run as on Fig. 8a).

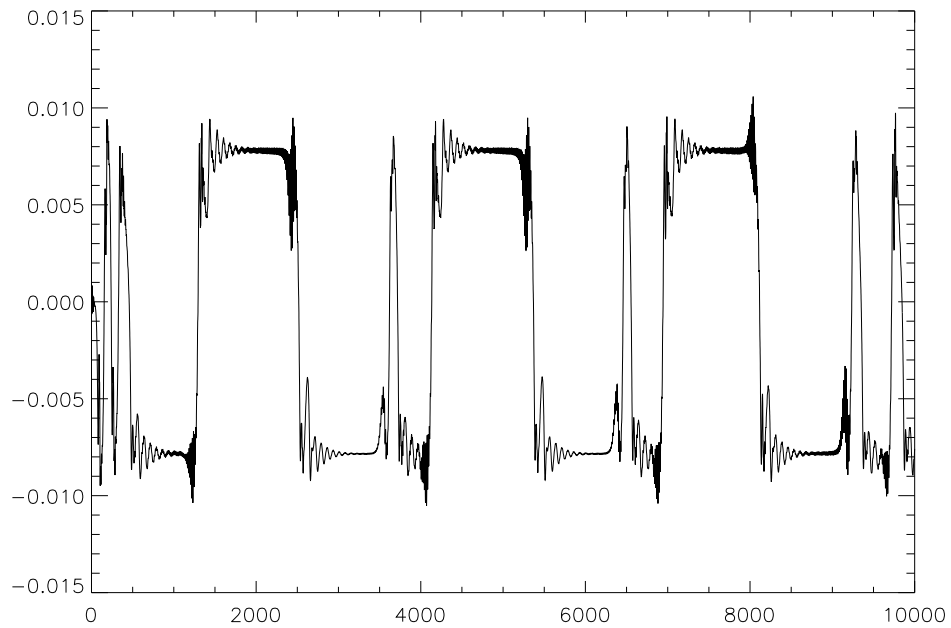


Figure 9. Fourier coefficient $\text{Im } b_{0;1;2}^1$ (vertical axis) as a function of time (horizontal axis) for $R = 4$ and $R_m = 48$.

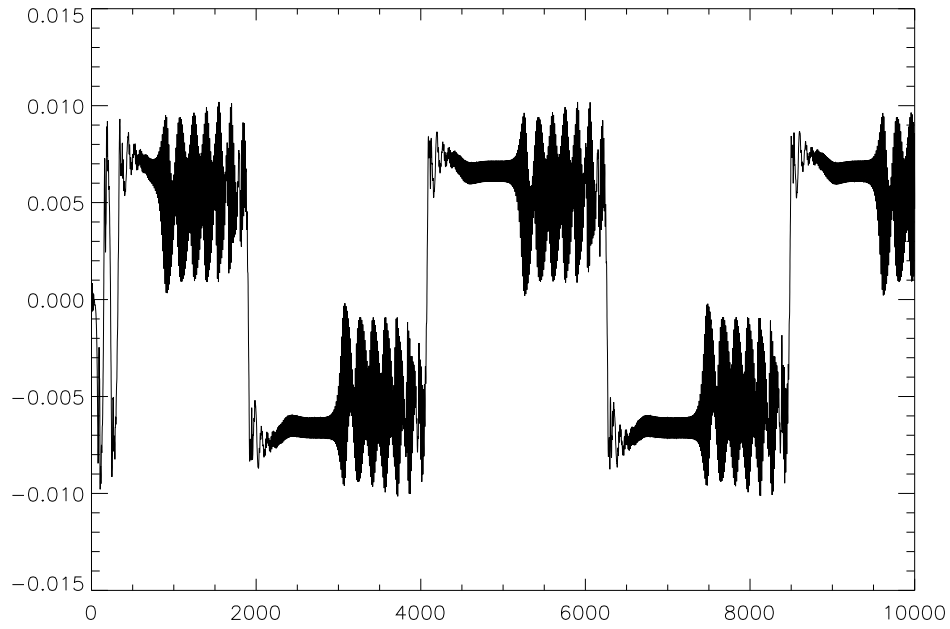


Figure 10a. Fourier coefficients $\text{Im } b_{0;l,2}^1$ (vertical axis) as a function of time (horizontal axis) for $R = 4$ and $R_m = 51$.

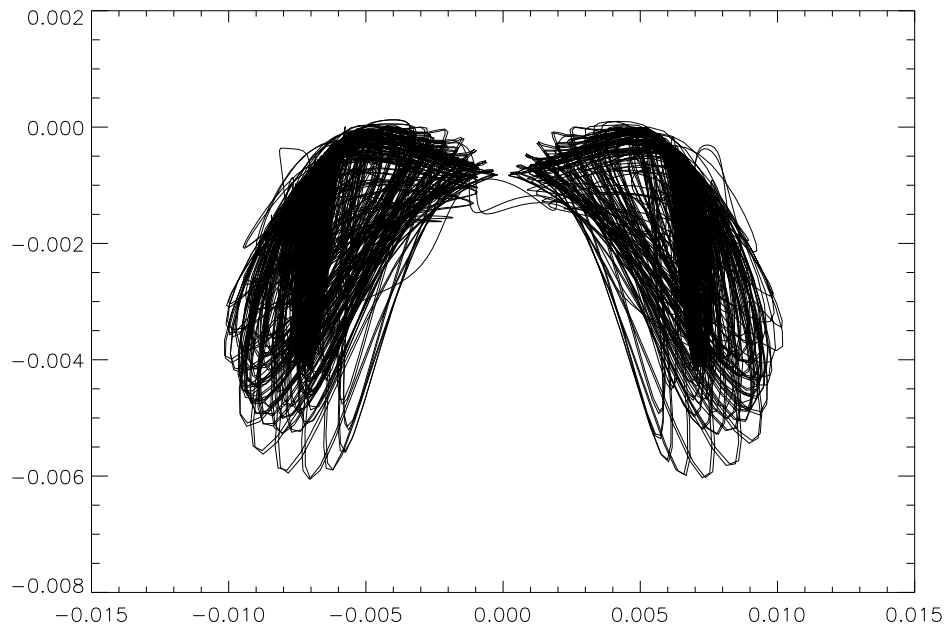


Figure 10b. Projection of the trajectory in saturated regime on the plane of Fourier coefficients $\text{Im } b_{0;l,2}^1$ (horizontal axis) and $\text{Re } v_{0;l,2}^1$ (vertical axis) for $R = 4$ and $R_m = 51$ (same run as on Fig. 10a).

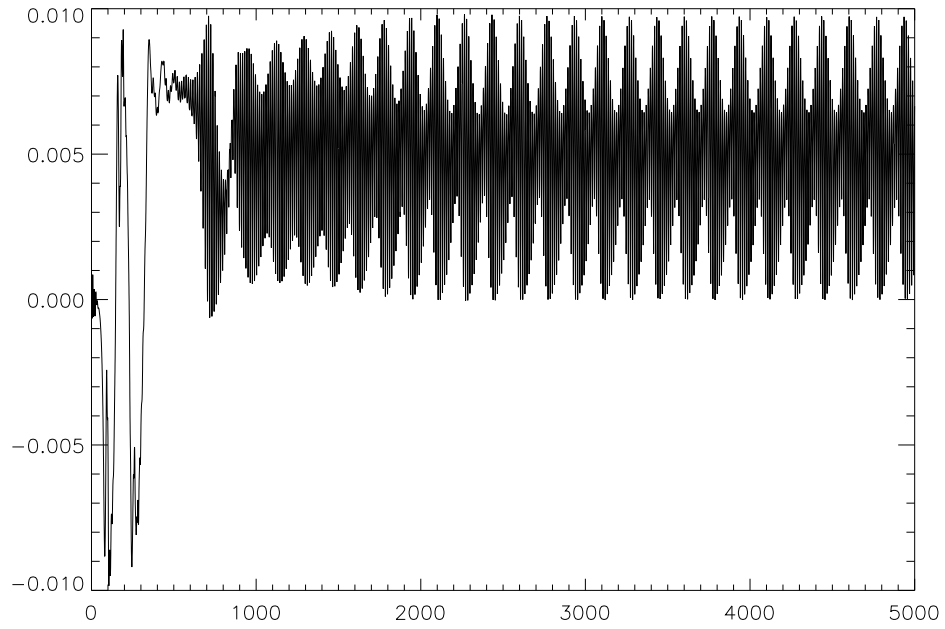


Figure 11a. Fourier coefficient $\text{Im } b_{0;1;2}^1$ (vertical axis) as a function of time (horizontal axis) for $R = 4$ and $R_m = 52$.

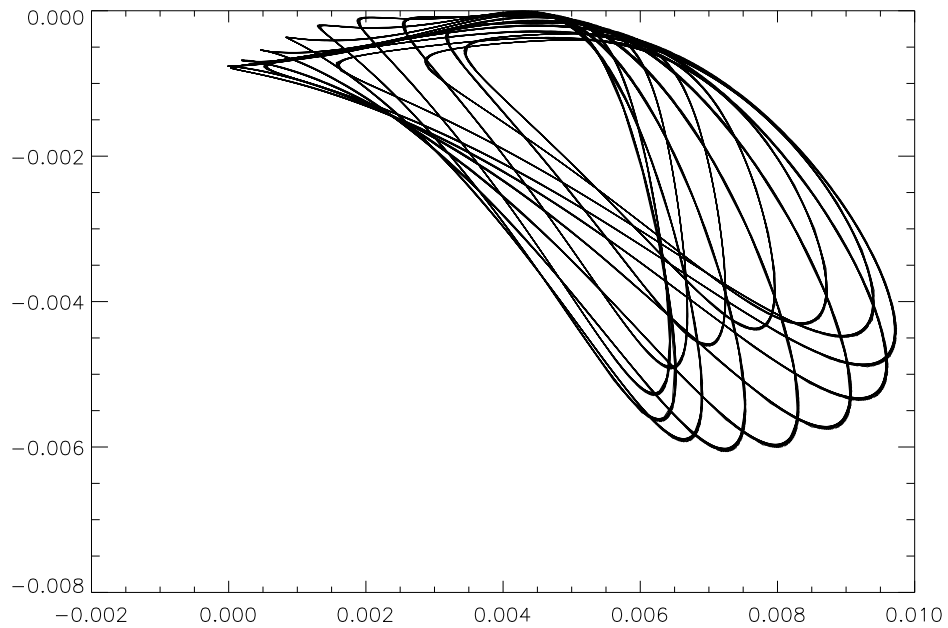


Figure 11b. Projection of the trajectory in saturated regime (tonus $T_{3;i}$) on the plane of Fourier coefficients $\text{Im } b_{0;1;2}^1$ (horizontal axis) and $\text{Re } v_{0;1;2}^1$ (vertical axis) for $R = 4$ and $R_m = 52$ (same run as on Fig. 11a).

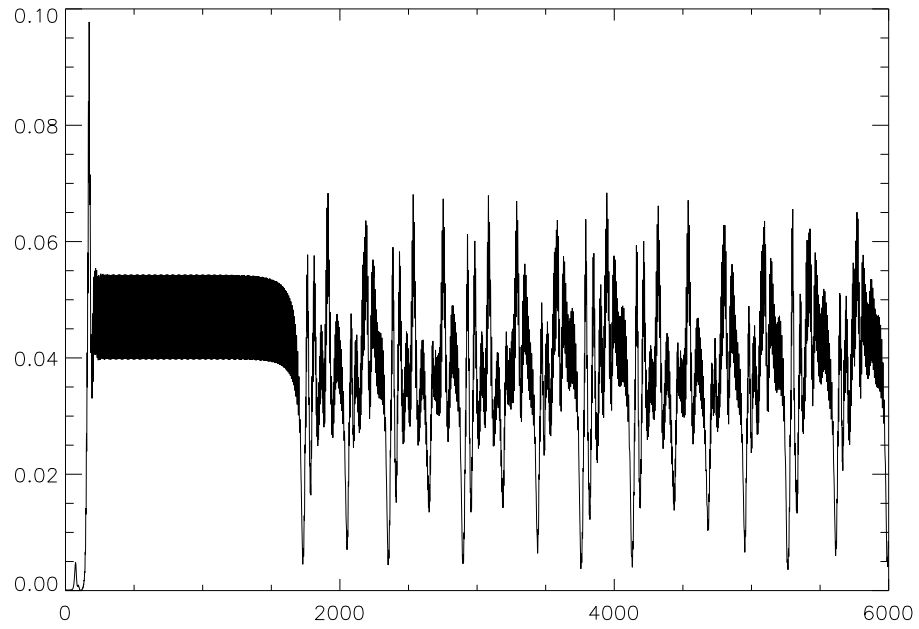


Figure 12. Magnetic energy (vertical axis) as a function of time (horizontal axis) for $R = 15$ and $R_m = 40$.

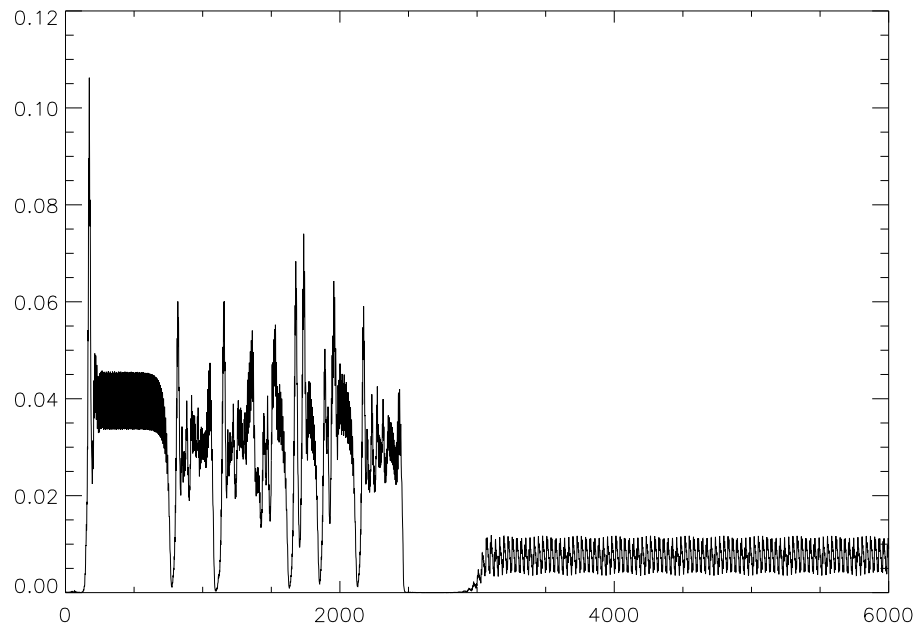


Figure 13. Magnetic energy (vertical axis) as a function of time (horizontal axis) for $R = 20$ and $R_m = 40$.

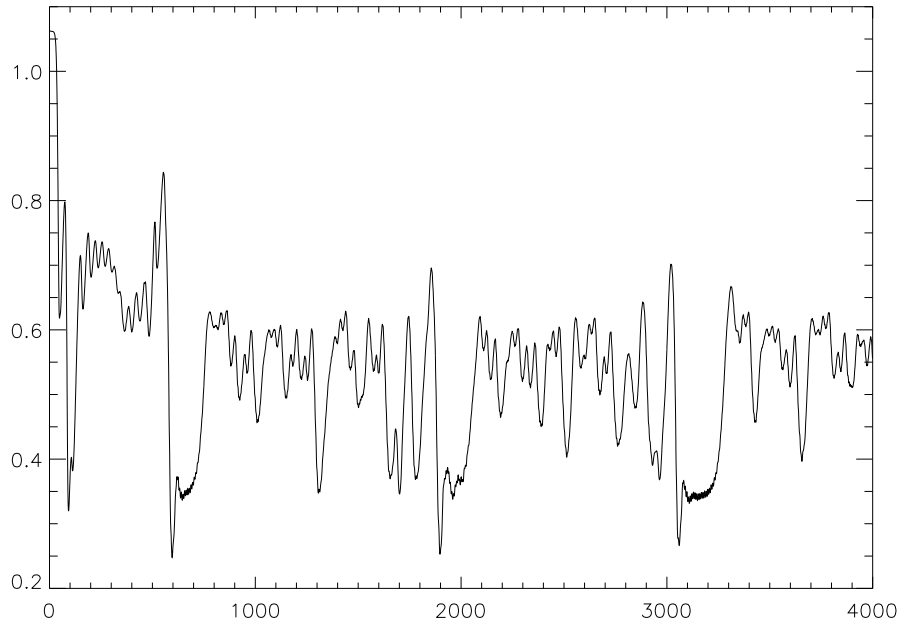


Figure 14a. Kinetic energy (vertical axis) as a function of time (horizontal axis) for $R = 25$ and $R_m = 40$.

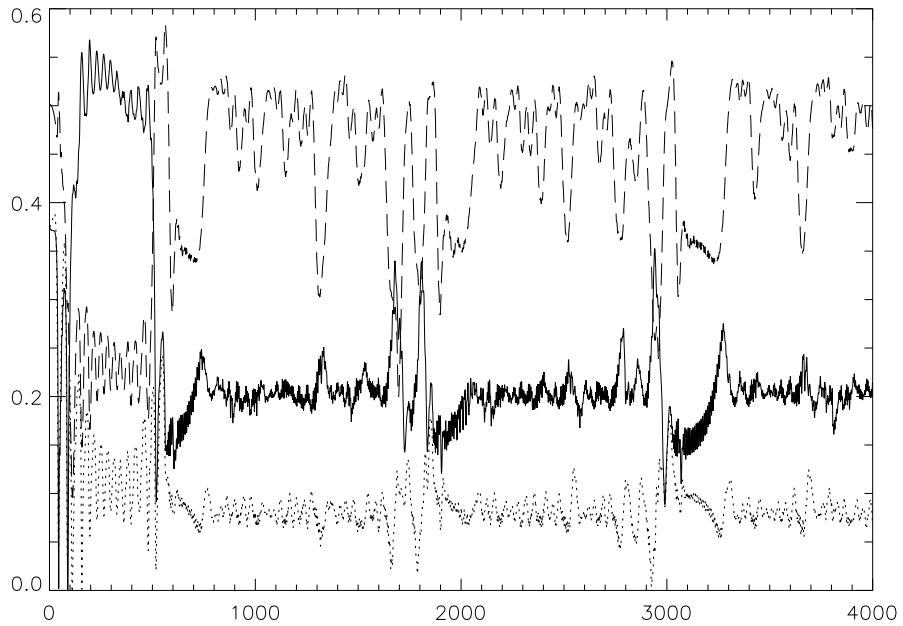


Figure 14b. Fourier coefficients of the flow (vertical axis: solid line $\{ \text{Rev}_{1,0;0}^3$, dashed line $\{ \text{Rev}_{0,1;0}^1$, dot line $\{ \text{Rev}_{0,0;1}^2$) as a function of time (horizontal axis) for $R = 25$ and $R_m = 40$ (same run as on Fig. 14a).

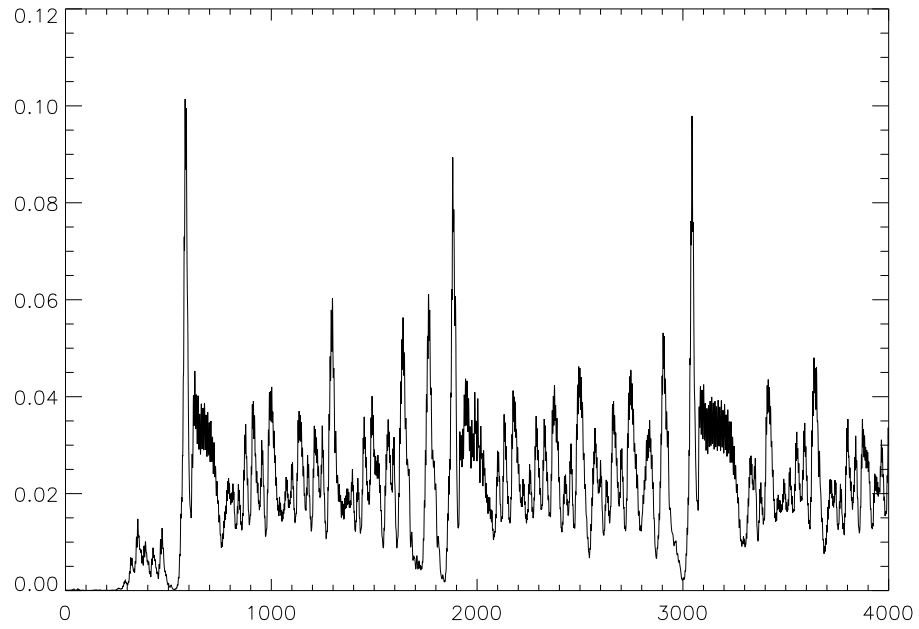


Figure 14c. Magnetic energy (vertical axis) as a function of time (horizontal axis) for $R = 25$ and $R_m = 40$ (same run as on Fig. 14a).

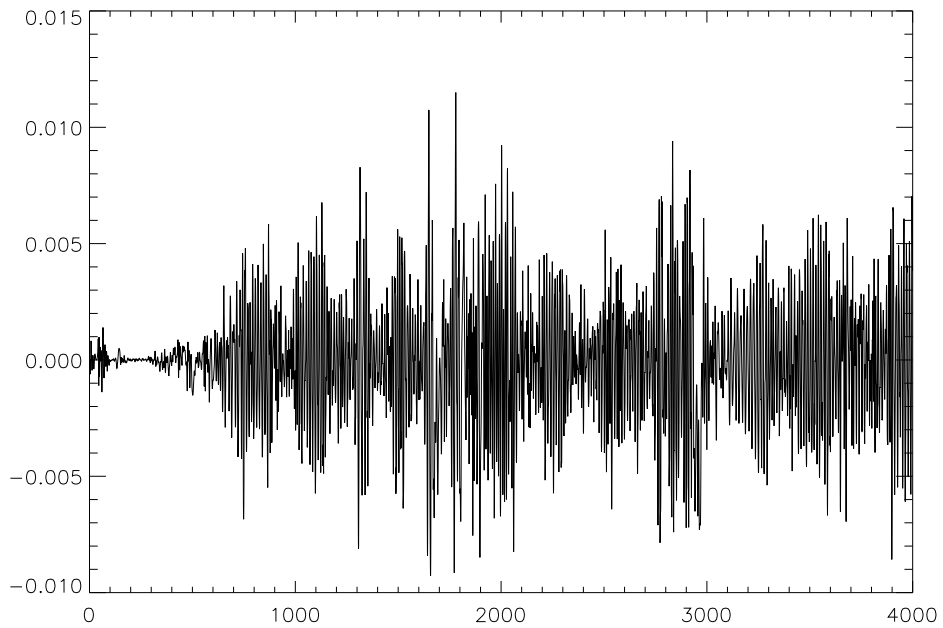


Figure 14d. Fourier coefficient $\text{Im } b_{0;1;2}^1$ (vertical axis) as a function of time (horizontal axis) for $R = 25$ and $R_m = 40$ (same run as on Fig. 14a).

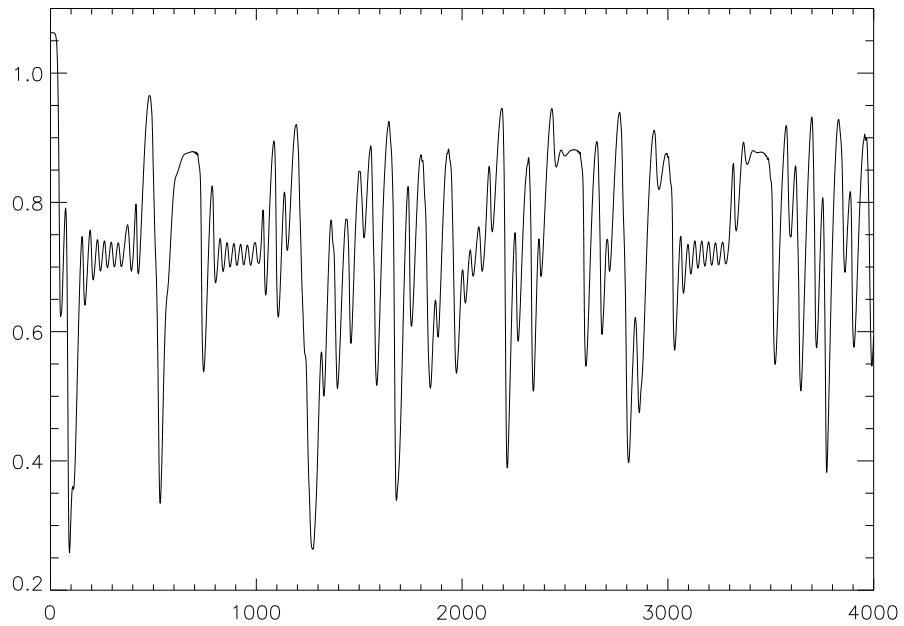


Figure 15a. Kinetic energy (vertical axis) as a function of time (horizontal axis) for $R = 25$ in the hydrodynamic problem (the initial condition for the flow is the same as on Fig. 14).

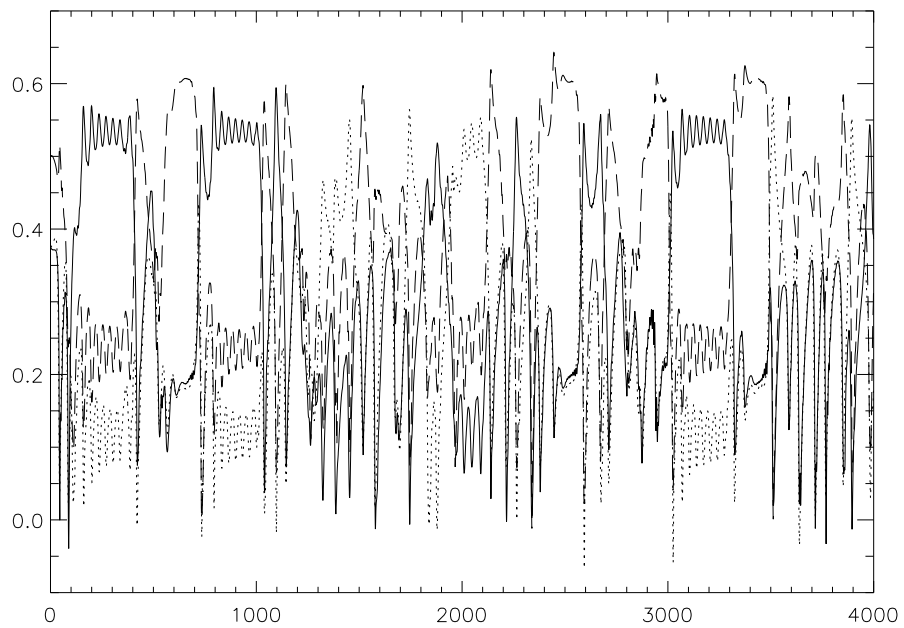


Figure 15b. Fourier coefficients of the flow (vertical axis: solid line $\{ \text{Rev}_{1,0;0}^3$, dashed line $\{ \text{Rev}_{0,1;0}^1$, dot line $\{ \text{Rev}_{0,0;1}^2$) as a function of time (horizontal axis) for $R = 25$ (same run as on Fig. 15a).

